RSC Advances

ROYAL SOCIETY OF CHEMISTRY

www.rsc.org/advances

Removal of phosphate from aqueous solution by SiO_2-biochar nanocomposites prepared by pyrolysis of vermiculite treated algal biomass

Yu-Ying Wang[1,2], Hao-Hao Lu[1,2], Yu-Xue Liu[1,2], Sheng-Mao Yang[1,2*]

[1] Institute of Environment, Resource, Soil, and Fertilizer, Zhejiang Academy of Agricultural Sciences, Hangzhou, 310021, P. R. China

[2] Engineering Research Center of Biochar of Zhejiang Province, Hangzhou, 310021, P. R. China

* Corresponding author:

Email: yangshengmao@263.net

Tel.: +86 571 86419218

Fax: +86 571 86419218

Abstract

The present work describes the fabrication of SiO_2-biochar nanocomposites by pyrolysis of vermiculite treated algal biomass. Physicochemical properties of the SiO_2-biochar nanocomposites were studied systematically by X-ray diffraction (XRD), Fourier transform infrared spectroscopy (FT-IR), scanning electron microscopy (SEM), and energy-dispersive X-ray analysis (EDX). Structure and morphology analysis of the sample showed that the SiO_2 particles were nanosized and uniformly formed on the carbon surface of the biochar. Effects of initial phosphate concentration, contact time, and pH on the adsorption capacity of SiO_2-biochar nanocomposites were investigated in detail. Adsorption experiments revealed that the initial pH of solution could affect the adsorption of phosphate onto the SiO_2-biochar nanocomposite. Of the mathematical models used to describe the adsorption kinetics of phosphate removal by the biochars, the pseudo-second-order model showed the best fit. Langmuir isotherm fitted the experimental data of phosphate adsorption onto the biochars better than the Freundlich and Redlich-Peterson adsorption model. Compared to the unmodified biochar, the SiO_2-biochar nanocomposite showed much greater ability to remove phosphate from aqueous solution, probably because the SiO_2 particles on the carbon surface served as sorption sites through electrostatic interactions. In addition, the adsorbed SiO_2-biochar nanocomposites could be effectively regenerated by NaOH solution. Our results suggest that SiO_2-biochar nanocomposites converted from vermiculite-treated algal biomass are promising alternative adsorbents, which can be used to reduce phosphate from water.

Keywords: Biochar, Vermiculite, SiO_2, Nanocomposite, Phosphate

1. Introduction

Anthropogenic eutrophication of water-supply reservoirs is one of the most prevalent environmental problems responsible for the degradation of water quality worldwide.[1-4] Eutrophication is mainly attributed to the addition of the nutrients (mainly phosphorus and nitrogen compounds) from point sources (usually sewage discharge) or from diffuse sources (such as agriculture and other anthropogenic activities) to the drainage basin.[4,5] Eutrophication increases the growth potential of phytoplanktons, such as harmful algae,[6] leading to harmful algal blooms (HABs). In these nutrients, phosphorus (P) is present mostly as phosphates[7] derived from several consumer products. Colloidal phosphate particles are discharged from industries involved in the production of fertilizers, detergents, pigment formulation, water treatment, and mineral processing.[8] Phosphate might pose a great threat for environmental health.[9,10] Being a growth limiting nutrient, high level of phosphate can promote excessive production of photosynthetic aquatic microorganisms in natural water bodies and can ultimately become a major factor in eutrophication of many freshwater and estuary coast ecosystems.[11] It is, therefore, very important to develop effective techniques for removal of phosphate from aqueous solutions prior to their discharge into the runoff and natural water bodies. To date, chemical precipitation, biological P uptake, and adsorption methods have been developed for removal of P from aqueous solutions prior to their discharge.[12-14] However, chemical precipitation process requires expensive chemicals and produces large amount of chemical sludge.[15] Biological P uptake could be limited because of the lack of carbon source and the difficulty in culturing microorganisms.[16] In contrast, removal of P by adsorption has advantages of easy control and less consumption.[17]

Recently, the application of biochar as a low-cost and environment-friendly adsorbent has been attracting attention, especially in phosphate removal studies. Biochar is a heterogeneous carbonaceous material and usually has large surface area, highly developed porosity, good ion exchange capacity, and high degree of surface reactivity.[18] Because of its potential in many environmental applications, including carbon sequestration, soil improvement, water treatment, and environmental remediation, biochar has received ample attention recently.[18-21] The porous structure, large surface area, and abundant oxygen-containing functional groups like carboxyl (-COOH) and hydroxyl (-OH)[22] have

helped biochar emerge as an important low-cost adsorbent that can be used to remove chemical contaminants including heavy metals, organic compounds, and other environmental pollutants.[23-28] Nowadays, the use of biochar to remove phosphate from aqueous solutions has become fascinating. However, owing to predominantly negatively charged surface of most of the biochars,[5,29] their sorption of anionic phosphate is relatively low.[5,9,30,31] For instance, Yao et al. observed that most of the thirteen biochars obtained from different biomass feedstocks had almost no ability to remove phosphate from aqueous solutions.[5] Chen et al. discovered that the P adsorption capacity of magnetic biochars made from iron-treated orange peel powders was only approximately 1.2 $mg \cdot g^{-1}$.[31] Namasivayam et al. and Bhargava and Sheldarkar reported that the P adsorption capacity of activated carbons derived from coir pith and tamarind nut shell was only approximately 5.1 and 5.0 $mg \cdot g^{-1}$, respectively.[9,30] Several methods have, therefore, been adopted to modify biochar for enhancing its sorption ability of phosphate.[32] For example, Fang et al. developed calcium and magnesium loaded biochar (Ca–Mg/biochar) and employed them for P recovery from biogas fermentation liquid.[21] Their results demonstrated that the maximum P adsorption of Ca–Mg/biochar was 326.63 $mg \cdot g^{-1}$.[21] Wang et al. produced biochar from oak sawdust by Lanthanum (La)-involved pyrolysis, the maximum PO_4^{3-} adsorption capacity of La-biochars was greatly improved (142.7 $mg \cdot g^{-1}$) compared with that of CK-biochars (32.0 $mg \cdot g^{-1}$).[28] Zhang and Gao successfully produced biochar/AlOOH nanocomposite with nanosized polycrystalline AlOOH flakes on biochar surface through thermal pyrolysis of $AlCl_3$ pre-treated biomass, and reported that this nanocomposite was a very attractive and high efficiency adsorbent for treatment of phosphate with a Langmuir maximum capacity of around 13.5 $mg \cdot g^{-1}$.[32] However, the methods used to synthesize these biochar nanocomposites are relatively complex and costly. Therefore, further investigations are necessary to develop simple and cost-effective methods to modify biochars with natural minerals.

The main objective of the present work was to develop and evaluate a new cost-effective method for preparation of biochar composites from algal biomass and natural clay mineral (vermiculite). The algal biomass, a by-product of eutrophication, was selected as the raw material for carbonization, to promote waste recycling. Vermiculite, a very common naturally occurring material is a 2:1 type layered clay mineral, which is relatively cheap and

eco-friendly.[33] It is mostly used as a low-cost refractory material for construction and soil amendment etc. Vermiculite-treated algae were used as the feedstock to produce the biochar through pyrolysis. As a result, a novel SiO_2-biochar nanocomposite was produced through thermal pyrolysis of vermiculite-treated algae. Considering the non-toxicity and chemical stability of SiO_2, the SiO_2-biochar nanocomposite exhibits a great potential as an adsorption material. Physicochemical properties of the resulting biochar were measured in laboratory and sorption ability of the biochar to phosphate was assessed through sorption experiments. The novel SiO_2-biochar nanocomposite demonstrated excellent adsorption ability for phosphate and, thus, can be used as a promising alternative adsorbent to remove phosphate from aqueous solutions to reduce eutrophication of fresh water. In addition, the P-laden biochar can also probably be recycled directly to soils as an effective slow-release P fertilizer.

2. Materials and methods

2.1 Materials

All chemicals including KH_2PO_4, HCl, NaOH, NaCl, $NaNO_3$, and $NaHCO_3$ employed in the experiments were of analytical reagent grade and were used without any further purification. Vermiculite was analytical reagent grade and purchased from Sigma-Aldrich. The crystalline silica in the vermiculite was in varying amounts (typically less than 1% crystalline silica). Phosphate solutions were prepared by dissolving monobasic potassium phosphate (KH_2PO_4) in deionized water.

2.2 Preparation of pristine biochar (BC) and vermiculite-modified algal biochar (VBC)

Algae, collected from Dongtou district, China, were used as precursors for biochar production. The feedstocks were dried in an oven at 75 °C for 24 h, milled to <0.5 mm size particles, and stored in airtight plastic containers until further use. Vermiculite was first immersed in 150 mL HCl (10%) for 24 h, and then filtered through 0.22 μm pore size filter membranes. This treated vermiculite can also be utilized as an adsorbent or for other purpose. Thereafter, 10 g of the feedstock was immersed in the filtrate solution for 24 h, and was

subsequently filtered. The pre-treated algae were oven dried at 80 °C overnight and then pyrolyzed in a programmable tube furnace (Hangzhou Lan Tian Instrument Co., Ltd.) *in vacuo*. It has been reported that biochars have moderate production rate, number of oxygen-containing functional groups, and alkalinity at 500 °C.[34] Therefore, in this study, pyrolysis was performed at 500 °C and the temperature was increased at a rate of 25 °C/min. After attainment of the target temperature, the sample was kept in the operating furnace for 3 h (residence time). Thereafter, the biochars were removed from the furnace, cooled in a desiccator, weighed, and stored in airtight plastic containers, which were designated as VBC. In addition, the pristine biochar derived from algae was also prepared following the same procedure at 500 °C. The resultant biochar sample was referred to as BC.

2.3 Characterization of biochars

Scanning electron microscopy (SEM) was performed using a JEOL JSM-6700F Scanning Microscope (Japan) to compare the structure and surface characteristics of the biochars. Energy-dispersive X-ray spectroscopy (EDX) was employed for elemental composition analysis of the biochars. X-ray diffraction (XRD, Bruker D8 Advance) was carried out on a Bruker's D8 Advance X-ray diffractometer equipped with graphite monochromatized Cu Kα irradiation over a 2θ collection range of 10–70° to examine the possible crystalline structures of biochars. Fourier transform infrared spectroscopy (FT-IR) was used to identify the functional groups of biochars over a wavenumber range from 400 to 4000 cm^{-1} (Nicolet iS10). The BET-surface area, micropore volume, and average pore width were measured with Nova2000e (Quantachrome, USA) using N_2 adsorption method. The zeta potential was obtained by adding approximately 0.1 g biochar to 50 mL deionized water. The suspensions were dispersed ultrasonically for 1 h in a sonicator, filtered, and the pH was adjusted so that it fell within a pH range of 2.0–8.0. The zero point charge of biochars was then determined using a particle analyzer (Nano ZS90).

2.4 Batch experiments

It is reported that municipal wastewater may contain 4 to 15 $mg \cdot L^{-1}$ phosphorus in the form of PO_4^{3-}. However, industrial wastewater (such as that derived from detergent manufacturing and metal coating processes) may contain phosphate levels much in excess of

10 mg·L^{-1}.[35] Therefore, the sorption ability of BC and VBC to phosphate was examined initially by adding 0.05 g of each sorbent to 50 mL phosphate aqueous solutions (10 or 50 mg·L^{-1}) in 100-mL conical flask at room temperature (25 ± 0.5 °C) for 24 h. The effect of pH on the removal ability of biochar was investigated in the pH range of 3.0 to 11.0. HCl (0.1 M) or NaOH (0.1 M) solution was used for initial pH adjustment of the phosphate solution. The characteristics and mechanisms of phosphate sorption onto BC and VBC were then investigated using sorption kinetic and isotherm experiments. For each experiment, 0.05 g of the sorbent was mixed with 50 mL phosphate solution in a conical flask. The mixture was then shaken on a thermostatically controlled shaker (ZWYR-2102C) at 120 rpm at room temperature. To measure the sorption kinetics, 10 or 50 mg·L^{-1} phosphate solutions were used at 10, 30, 60, 180, 300, 480, 720, and 1440 min range contact time intervals. To obtain sorption isotherms, 0.05 g biochar was mixed with 50 mL phosphate solution of different concentrations (0, 2, 5, 7, 10, 20, 25, 50, 70, and 100 mg·L^{-1}) in a batch of conical flask and shaken for 24 h. At the end of each experiment, the mixtures were immediately filtered through 0.22-μm pore size filter membranes. For the effect of ionic strength, the experiments were performed at pH 5.0 and 25 °C, and the initial phosphate solution (50 mg·L^{-1}) was adjusted to different concentrations of NaCl (0, 0.001, 0.005, 0.01, 0.05, 0.1, 0.5 mol·L^{-1}). Moreover, the effect of the common coexisting anions, chloride, nitrate, and bicarbonate, was also investigated by adding 0.01 M of NaCl, $NaNO_3$, or $NaHCO_3$ to the 50 mg·L^{-1} phosphate solutions in separate conical flasks. All the adsorption experiments were performed in triplicate to ensure reproducibility and the average experimental data are reported. Additional measurements were conducted whenever two measurements showed a difference larger than 5%.

2.5 Desorption experiment

The feasibility of regenerating SiO_2-biochar nanocomposite for repeated use was investigated by using sodium hydroxide (NaOH) as stripping agent. Desorption experiment was conducted as follows: the SiO_2-biochar nanocomposite, which had been used to remove phosphate (100 mg·L^{-1}) was added to 50 mL of 0.5 mol·L^{-1} NaOH solution, shaken at 120 rpm at 25 °C for 24 h. Thereafter, the SiO_2-biochar nanocomposite was collected, washed to

neutral pH by deionized water and dried for the next adsorption–desorption cycle.

2.6 Phosphate analysis

The phosphate concentration was analyzed using the ammonium molybdate spectrophotometric method[36] with a UV-6100 spectrophotometer at a wavelength of 700 nm. Adsorption efficiency (q_e) and uptake percentage (U%) were calculated by the following equations:

$$q_e = \frac{(C_o - C_e)V}{W}$$

$$U\% = \frac{(C_o - C_e)100\%}{C_o}$$

where, C_o and C_e ($mg \cdot L^{-1}$) are the initial and equilibrium concentration of phosphate. V (mL) is the total volume of the solution and W (mg) is the mass of the modified biochar.

3. Results and Discussion

3.1 Morphology and crystalline structure of the vermiculite-modified biochar

The structure and phase purity of the obtained biochar were first examined by XRD analysis. Typical XRD pattern of the vermiculite-modified biochar is shown in Figure 1a. Compared with the Joint Committee on Powder Diffraction Standards (JCPDS) file (No. 861630), these diffraction peaks could be indexed to hexagonal quartz with lattice parameters of a = 4.914 Å and c = 5.046 Å. The diffraction peaks at 20.8°, 26.6°, 36.5°, 39.5°, and 50.1° corresponded to five indexed planes (100), (101), (110), (012), and $(11\bar{2})$ of SiO_2, respectively. Therefore, SiO_2 was believed to be the major crystalline phase for the synthesized nanoparticles within the biochar nanocomposite. In addition, the strong and sharp XRD reflection peaks also confirmed that the as-prepared sample was well crystallized. The corresponding FT-IR spectrum is shown in Figure 1b. The very intense and broad band appearing at 1098 cm^{-1} was assigned to asymmetric stretching vibrations of Si–O–Si.[37] The bands at 803 and 477 cm^{-1} could be attributed to the characteristic symmetric stretching vibrating vibration absorption peaks of Si–O.[37] The peaks at 1098, 803, and 477 cm^{-1} agreed to the Si–O–Si bond, which implied the existence of SiO_2. This result was consistent with that

of XRD analysis presented in Figure 1a. Moreover, the broad band centered at 3420 cm^{-1} (between 3550 and 3200 cm^{-1}) was due to the stretching vibrating vibration absorption peaks of the hydrogen-bonded hydroxyl groups of water,[38] and the peaks at 1614 cm^{-1} corresponded to the flexural vibrating absorption peaks of physically absorbed water.[39]

The morphology and size of the vermiculite-modified biochar were also characterized by field emission scanning electron microscopy (FESEM). As shown in Figure 2a, the vermiculite-modified biochar was in the form of sheets and the surface of sheets was rough with nanoparticles present on it. The further magnified FESEM images represented in Figure 2b, c unambiguously reveal that the nanoparticles were homogeneously and densely grown on the biochar surface. Corresponding EDX analysis (EDX, Fig. 2d) demonstrated that nanoparticles on the biochar surface contained silicon and oxygen, as well as small amount of carbon, magnesium, aluminum, chlorine, potassium, and gold, where carbon and potassium came from biochar, magnesium, aluminum, and chlorine came from HCl-treated vermiculite solution, and gold from the sample preparation for SEM analysis, indicating that the nanoparticles on biochar surface should be silicon dioxide. Therefore, the XRD, FT-IR, and FESEM analyses clearly demonstrated that the SiO_2-biochar nanocomposite was successfully fabricated by pyrolyzing vermiculite-treated algal biomass in our experiment. Vermiculite is a very common naturally occurring material. After acid treatment, the structure of vermiculite was destroyed. When the algal feedstock was immersed in the filtrate, some amorphous silica was attached to the surface of algae. In the process of pyrolysis, SiO_2 was formed on the surface of biochar and SiO_2-biochar nanocomposite was produced.

In addition, mesoporous structure in biochars was demonstrated by gas sorption experiments according to Brunauer, Emmett, and Teller (BET). The representative N_2 sorption isotherm and the corresponding Barrett-Joyner-Halenda (BJH) pore size distribution curves are depicted in Figure 3a and b. The isotherm curve (Fig. 3a) showed hysteresis loops in the relative pressure (P/P_o) range from 0.4 to 0.9, demonstrating that the structures were uniform mesopores. The N_2 isotherm of both BC and VBC were type IV isotherm with a type H3 hysteresis loop, indicating that all the biochars had mesoporous structures.[40] Moreover, the BET surface area (BET), pore diameter (d), and total pore volume (Vtotal) of VBC were 42.43 $m^2 \cdot g^{-1}$, 5.17 nm, and 0.055 $cm^3 \cdot g^{-1}$, respectively; whilst those of BC were 8.07 $m^2 \cdot g^{-1}$,

11.70 nm, and 0.024 $cm^3 \cdot g^{-1}$, respectively. Obviously, there was a significant increase in the BET surface area and total pore volume for VBC, as compared to BC, which was expected to benefit the phosphate adsorption process. Furthermore, the pore size distribution curves of the biochars (Fig. 3b) were determined from the adsorption branch of the isotherm. The pore size distribution peaks were centered at 6.0 and 4.1 nm for BC and VBC, respectively. The surface area analysis further confirmed the nano-porous structures of the SiO_2-biochar nanocomposites. These results suggested that SiO_2-biochar nanocomposites derived from algae had high surface areas and micropores, and could, therefore, be used as potential adsorbent for water treatment or environmental remediation.

3.2 Sorption of BC and VBC to phosphate

3.2.1 Influence of pH

Influence of pH of the medium on the uptake is important in view of practically assessing the efficacy in real wastewater systems, which vary depending on the source. Phosphate exists as different species at different pH of the solution. Therefore, pH affects not only the surface charge of the biochars, but also the degree of ionization and speciation of the phosphate in solution. Here, the influence of pH on the removal efficiency of phosphate was investigated. Figure 4 shows the effect of pH on the removal efficiency of phosphate in the 3.0 to 11.0 range. The initial pH values were adjusted before the addition of biochar into the solution by HCl or NaOH. The phosphate concentration was set as 10 (Fig. 4a) and 50 $mg \cdot L^{-1}$ (Fig. 4b), respectively, and the agitation time was 24 h. As shown in Figure 4, the adsorption process of phosphate was strongly dependent on the pH of the solution. The uptake percentage of phosphate adsorption was sharply increased when the pH of solution increased from 3.0 to 5.0. At pH > 8.0, a gradual decrease was observed in the uptake percentage. When the pH reached 9 and 11.0, the uptake percentage of phosphate adsorption was decreased further. Similar findings have been reported in the literature, including the work of de Vicente et al., who showed that the percentage of removal of phosphate by iron particles was 98% at pH 5 and 6, which decreased to 88% at pH 7 and 82% at pH 8–9.[41] Considering the dissociation constants of phosphoric acid (pKa1 = 2.15, pKa2 = 7.20, pKa3 = 12.33), phosphate acid can dissociate to form different ionic species depending on the pH of the

solution ($H_2PO_4^-$, HPO_4^{2-}, and PO_4^{3-}).[42] When the pH increased from 3 to 7, $H_2PO_4^-$ was the superior form in the solution, whereas HPO_4^{2-} was the superior form in the solution when the pH increased from 7 to 10. In the pH range of 3.0–7.0, the relatively high uptake percentage of removal of phosphate was observed. This was because the SiO_2 nanoparticles deposited on the biochar surface acted as active sites, providing great affinity to $H_2PO_4^-$. Nevertheless, a subtle decrease in the uptake was observed at higher pH (8–11), probably ascribed to an increase in the electrostatic repulsion between the phosphate anion with the negatively charged surface as well as the competition by hydroxide ion with phosphate anion as the charge neutralizing species. This result would be further confirmed by the point of zero charge of biochars. Zeta potential is the potential of a sliding plane of colloidal particles, and its value and sign are related to surface charge of the particles that depends on the pH of the solution.[43] The zeta potential can reflect adsorption properties of biochars.[44] The point of zero charge (pHpzc) is the pH at which the net charge on the surface is zero. The zeta potentials of the pristine biochar and SiO_2-biochar nanocomposite (BC and VBC) were shown in Figure 5. The pHpzc of the BC and VBC was found to be at pH 4.6 and 4.8, respectively. Under the solution pH < pHpzc, the surface of the biochars was positively charged, which could lead to a significant electrostatic attraction between the phosphate and the positively charged surface. When the solution pH > pHpzc, the surface of the biochars acquired a negative charge, which did not favor the phosphate adsorption due to electrostatic repulsion.[45] In our experiment, the relatively high uptake percentage of removal of phosphate was observed in the pH range of 3.0–7.0 and a subtle decrease in the uptake was observed at higher pH (8–11). Therefore, in the subsequent experiments, pH was set at 5.

3.2.2 Adsorption kinetics

To explain the mechanism of adsorption processes, pseudo-first-order and pseudo-second-order models were applied to simulate the experimental kinetic data. The equations for these models are generally expressed as follows:

$$\log(q_e - q_t) = \log q_e - \frac{tk_1}{2.303}$$

$$\frac{t}{q_t} = \frac{1}{k_2 q_e^{\ 2}} + \frac{t}{q_e}$$

where, q_e and q_t ($mg \cdot g^{-1}$) represent the sorption amount of phosphate at equilibrium and at time t, and k_1 (min^{-1}) and k_2 ($g \cdot mg^{-1} \cdot min^{-1}$) are the pseudo-first-order and pseudo-second-order reaction rate constant, respectively (Table 1). The pseudo-second-order model assumes that the rate-limiting step might be the chemical adsorption.[46]

The effect of contact time on phosphate adsorption by BC and VBC at initial phosphate concentration of 10 and 50 $mg \cdot L^{-1}$ is represented in Figure 6a and b, respectively. As plotted in Figure 6a, when the concentration of phosphate was 10 $mg \cdot L^{-1}$, it could be removed nearly completely by SiO_2-biochar nanocomposite (VBC) in 12 h, indicating high removal efficiency of VBC for phosphate. The removal efficiency was also dramatic in the experiment carried out with the more concentrated initial solution containing 50 $mg \cdot L^{-1}$ phosphate, but in this case, it was observed after 5 h equilibration. Moreover, in both the cases, the removal efficiency of phosphate by VBC was higher than by pristine biochar (BC). The kinetic data recorded in the phosphate solution with different initial concentrations fitted into both the pseudo-first-order and pseudo-second-order models (Fig. 7 and 8); the corresponding parameters and correlation coefficients are listed in Table 1. The results were found to better match with the pseudo-second-order model (R^2 = 0.999) rather than the pseudo-first-order model, suggesting that the adsorption process was chemisorption. Furthermore, the value of the calculated equilibrium adsorption capacity ($q_{e,cal}$) of phosphate calculated from the pseudo-first-order kinetic model did not give reasonable values, which were much lower than the experimental $q_{e,exp}$ value, indicating that the phosphate adsorption process of BC and VBC was not determined by physical adsorption. However, the value of the equilibrium adsorption capacity ($q_{e,cal}$) of phosphate, calculated from pseudo-second order model, was close to the experimental $q_{e,exp}$ value. Therefore, the adsorption process was better represented by the pseudo-second order model, indicating that the chemisorptions of phosphate on SiO_2-biochar were the rate-limiting mechanism.[47] Phosphate ions were adsorbed onto the surface of SiO_2-biochar by chemical interaction, such as ion exchange and chelating reaction.[48] Similar results were observed for phosphate adsorption onto the other adsorbents, such as lanthanum-doped mesoporous silicates,[49] hydrated ferric oxide doped activated carbon,[50] and

magnetic iron oxide nanoparticles.[51] In particular, the rate constants (k) derived from the adsorption kinetic data using VBC in the solution with initial concentrations of 10 and 50 $mg \cdot L^{-1}$ were 0.0056 and 0.0027 $g \cdot mg^{-1} \cdot min^{-1}$, respectively. It revealed that VBC possessed a faster removal rate at a higher concentration; therefore, shorter time was required for the attainment of equilibrium. As seen in Figure 6, in 10 $mg \cdot L^{-1}$ phosphate solution, the adsorption equilibrium was reached within 12 h; whereas in 50 $mg \cdot L^{-1}$ phosphate solution, the equilibrium was attained within 5 h. This means that low-concentration phosphate was harder to remove.

3.2.3 Adsorption isotherms

The equilibrium adsorption isotherms are essential data to explain the mechanism of adsorption. Non-linear regression analysis of three isotherms, Langmuir, Freundlich, and Redlich–Peterson, was applied to the adsorption data obtained in the present work.

The Langmuir model is represented by the following equation:[52]

$$q_e = \frac{K_L b C_e}{1 + b C_e}$$

where, q_e ($mg \cdot g^{-1}$) denotes the amount of phosphate adsorbed at equilibrium adsorption capacity, C_e ($mg \cdot L^{-1}$) is the equilibrium concentration of phosphate in solution, and K_L and b are the Langmuir constants related to the adsorption capacity and energy of adsorption, respectively.

The Freundlich model is represented by the following equation:[53]

$$q_e = K_F C_e^{1/n}$$

where, q_e ($mg \cdot g^{-1}$) is the adsorption capacity at equilibrium, C_e ($mg \cdot L^{-1}$) is the equilibrium concentration, K_F ($mg \cdot g^{-1}$)($L \cdot mg^{-1}$)$^{1/n}$ is the Freundlich constant, related to adsorption capacity, and 1/n is an empirical constant indicating the intensity of the adsorption.

Redlich-Peterson isotherm model is represented by the following equation:[54]

$$q_e = \frac{K_R C e}{1 + a_R C_e^{\beta}}$$

where, q_e is the solid phase sorbate concentration at equilibrium ($mg \cdot g^{-1}$), C_e is the liquid

phase sorbate concentration at equilibrium ($mg \cdot L^{-1}$), K_R is a Redlich–Peterson isotherm constant ($L \cdot g^{-1}$), a_R is a Redlich–Peterson isotherm constant ($L \cdot mg^{-1}$), and β is the exponent, which lies between 1 and 0. If β = 1, Langmuir is the preferred isotherm, if β = 0 then Freundlich is the preferred isotherm.

The proper constants together with correlation coefficients are presented in Table 2, whereas the comparison of the applied isotherms is shown in Figure 9. It can be seen that all the applied sorption models resulted in nonlinear curve, although the agreement of the experimental data with the models was good. Among these models, the best interpretation of the experimental data was shown by the Langmuir isotherm (R^2 = 0.977 and 0.979 for BC and VBC, respectively) compared to the other two isotherms. Moreover, the Freundlich equation (R^2 = 0.954 and 0.955 for BC and VBC, respectively) gave a relatively better interpretation of the experimental data than the Redlich-Peterson model (R^2 = 0.758 and 0.917 for BC and VBC, respectively). It means that the monolayer coverage of phosphate onto both BC and VBC is feasible. Furthermore, according to the Langmuir isotherm model, the removal capacity of phosphate by BC and VBC were approximately 98.2 and 159.4 $mg \cdot g^{-1}$, respectively. The maximum capacity for phosphate adsorption of the SiO_2-biochar nanocomposites (VBC) was approximately 1.6-folds higher compared to that of the pristine biochar (BC). As revealed by the adsorption kinetic study, the adsorption of phosphate on both BC and VBC was better represented by the pseudo-second order model. This indicates that the adsorption was a result of chemical sorption. Moreover, from the FESEM images (Figure 2), the SiO_2 nanoparticles were homogeneously and densely grown on the biochar surface. Therefore, the SiO_2 nanoparticles on the surface of biochar can play an important role on the phosphate adsorption. The SiO_2 nanoparticles on the surface of biochar served as sorption sites and adsorbed phosphate through electrostatic interactions leading to a greater ability for removal of phosphate from aqueous solution compared to the unmodified biochar. Furthermore, the removal capacity was higher than that of the previously reported adsorbents, such as Fe–Cu binary oxide,[55] La-doped vesuvianite,[56] mesoporous ZrO_2,[57] ACF-NanoHFO,[50] biochar/AlOOH nanocomposite,[32] magnetic iron oxide nanoparticles,[51] and biochar derived from digested sugar beet tailings,[58] as summarized in Table 3. The SiO_2-biochar nanocomposites showed much greater ability to remove phosphate from aqueous solution,

probably because the SiO_2 particles on the carbon surface served as sorption sites through electrostatic interactions. Therefore, the remarkably high performance of SiO_2-biochar nanocomposite in the removal of phosphate could be attributed to its unique carbon-nanoparticle structure, which dramatically increased the reactive area and sites to attract the contaminants from water. The SiO_2-biochar nanocomposite is an attractive and high efficiency adsorbent for the treatment of phosphate-polluted water.

3.2.4 Effect of ionic strength studies

NaCl, a common salt, was selected to study the influence of ionic strength on phosphate removal. The ionic strengths were adjusted by 0, 0.001, 0.005, 0.01, 0.05, 0.1 and 0.5 $mol \cdot L^{-1}$ NaCl solutions at room temperature. As shown in Figure 10, the presence of NaCl has a little influence on phosphate removal at low concentrations (0.001 and 0.005 $mol \cdot L^{-1}$). However, the removal capacity of phosphate was obviously reduced from approximately 98% to 70% and 51% at higher NaCl concentrations (0.1 and 0.5 $mol \cdot L^{-1}$). This is because Na^+ and Cl^- are monovalent ions and could not or only slightly compete for the adsorption site of SiO_2-biochar nanocomposite at low concentration.[43,59] In contrast, at high concentrations, the presence of Cl^- and Na^+ could hinder the electrostatic interaction between SiO_2-biochar nanocomposite and phosphate in solution and could also compete with the phosphate for surface adsorption sites of the SiO_2-biochar nanocomposite.

3.2.5 Effect of coexisting anions in solution

The anions, chloride, nitrate, and bicarbonate, are common in natural waters and can compete with phosphate for surface active sites of the adsorbent. Therefore, studying the adsorption preference of SiO_2-biochar nanocomposite toward phosphate in the presence of coexisting anions is important. The effects of Cl^-, NO_3^- and HCO_3^- on phosphate uptake by the SiO_2-biochar nanocomposite are shown in Figure 11. It can be observed that Cl^- and NO_3^- had little effect on the adsorption of phosphate (approximately 4.5 percent decrease) onto the SiO_2-biochar nanocomposite (Fig. 11), suggesting low competitions between phosphate and these two ions. However, the existence of HCO_3^- in the solution reduced the phosphate adsorption by approximately 39.4%. This indicated that HCO_3^- would compete for the

adsorption site with phosphate.

3.3 Regeneration and desorption analysis

Desorption is another important process reflecting adsorption due to its economical and enhancement value. Here, the regeneration of the SiO_2-biochar nanocomposite was investigated by using 0.5 mol·L^{-1} NaOH desorption. As shown in Figure 12a, the adsorption ability of the SiO_2-biochar nanocomposite decreased gradually with the increasing number of cycles, but the percentage of removal of phosphate was no less than 75% in the fifth cycle. This suggested that SiO_2-biochar nanocomposite can be regenerated effectively using NaOH solution. The decreasing adsorption ability could be assigned to the wastage of the adsorbent during the process. Furthermore, the morphology of the SiO_2-biochar nanocomposite after recycling was also characterized by FESEM. As shown in Figure 12b, the SiO_2-biochar nanocomposite was still in the form of sheets after recycling. Moreover, the surface of sheets was still rough and the SiO_2 nanoparticles were also present on the biochar surface. Therefore, the SiO_2 nanoparticles were stable on the biochar surface even after reuse for five cycles.

It is well known that biomineralization is a process by which living organisms produce organic/inorganic composites, often to harden or stiffen their existing tissues. Silica (biosilica) is the second-most abundant constituent of biominerals after carbonate. Biosilica has attracted much attention because of its unique morphology and hierarchical structures, fascinating mechanical properties, and potential applications in many fields. For instance, silica may be an ideal material for grafting and scaffolding.[60] Introduction of nano-sized silica particles into polymeric materials can not only endow polymer scaffolds with biomineralization capability but also increase the stiffness of polymer material without greatly decreasing the mechanical strength.[61] Moreover, silica derivatives have been introduced as bone substitutes,[62] with good clinical success rates and promotion of new vital bone formation around these materials[63] and as bio-mimetic agents to coat implant surfaces.[64] In addition, SiO_2 has been widely used in the environment. For example, Li et al. fabricated carbon/SiO_2 composites from hydrothermal carbonization and found that the composites had high adsorption efficiency for Pb^{2+}.[65] Chen et al. synthesized the core–shell magnetic γ-Fe_2O_3/SiO_2 nanocomposite and found that the γ-Fe_2O_3/SiO_2 nanocomposite exhibited high adsorption capacity for removing

methylene blue from water.[66] Therefore, silica has been reported to be a nontoxic, environmental material and the SiO_2-biochar nanocomposite obtained in our experiment can be used as effective adsorbent in the environment.

4. Conclusions

A SiO_2-biochar nanocomposite was successfully synthesized by pyrolyzing vermiculite treated algal biomass and was used as an effective adsorbent for phosphate. Compared to the pristine biochar, the SiO_2-biochar nanocomposites showed enhanced sorption of phosphate. The enhanced phosphate sorption by SiO_2-biochar nanocomposites was mainly due to the presences of SiO_2 particles on the surface of biochar, which served as sorption sites through electrostatic interactions, and thus played an important role in the sorption. The algal biomass is a by-product of eutrophication and vermiculite is a low-cost, abundant, and inexpensive natural material. Moreover, the treated vermiculite can also be recycled. Therefore, the SiO_2-biochar nanocomposites developed in the present work are cost-effective and helpful in waste recycling, and can be used as multifunctional and highly effective adsorbent to remove phosphate. In addition, the phosphate-laden biochar has an abundance of valuable nutrients and may be used as a slow-release fertilizer to enhance soil fertility and to sequester carbon.

Acknowledgements

This work was supported by the National Natural Science Foundation of China (Grant No. 41301247).

References

1 M. Genkai-Kato and S. R. Carpenter, *Ecology*, 2005, **86**, 210-219.

2 I. Kagalou, E. Papastergiadou and I. Leonardos, *J. Environ. Manage.*, 2008, **87**, 497-506.

3 P. M. Nyenje, J. W. Foppen, S. Uhlenbrook, R. Kulabako and A. Muwanga, *Sci. Total*

Environ., 2010, **408**, 447-455.

4 L. Wang, L. Liu and B. Zheng, *J. Environ. Sci.*, 2013, **25**, 962-970.

5 Y. Yao, B. Gao, M. Zhang, M. Inyang and A. R. Zimmerman, *Chemosphere*, 2012, **89**, 1467-1471.

6 J. Carstensen, P. Henriksen and A. S. Heiskanen, *J. Environ. Sci.*, 2007, **52**, 370-384.

7 T. C. Chen, Y. J. Shih, C. C. Chang and Y. H. Huang, *J. Taiwan. Inst. Chem. E.*, 2013, **44**, 61-66.

8 M. Özacar, *J. Hazard. Mater.*, 2006, **137**, 218-225.

9 D. S. Bhargava and S. B. Sheldarkar, *Water Res.*, 1993, **27**, 325-335.

10 M. Özacar, *Chemosphere*, 2003, **51**, 321-327.

11 S. Karaca, A. Gürses, M. Ejder and M. Acikyildiz, *J. Colloids Interface Sci.*, 2004, **277**, 257-263.

12 P. H. Abelson, *Science*, 1970, **167**, 1081-1081.

13 M. S. Onyango, D. Kuchar, M. Kubota and H. Matsuda, *Ind. Eng. Chem. Res.*, 2007, **46**, 894-900.

14 J. L. Nielsen and P. H. Nielsen, *Environ. Sci. Technol.*, 1998, **32**, 3556-3561.

15 T. Zhang, P. Li, C. Fang and R. Jiang, Ecol. *Chem. Eng. S.*, 2014, **21**, 89-99.

16 B. E. Rittmann, B. Mayer, P. Westerhoff and M. Edwards, *Chemosphere*, 2011, **84**, 846-853.

17 Y. Yao, B. Gao, J. Chen and L. Yang, *Environ. Sci. Technol.*, 2013, **47**, 8700-8708.

18 M. Inyang, B. Gao, P. Pullammanappallil, W. Ding and A. R. Zimmerman, *Bioresour. Technol.*, 2010, **101**, 8868-8872.

19 J. Lehmann, J. Gaunt and M. Rondon, *Mitig. Adapt. Strat. Glob. Change*, 2006, **11**, 395-419.

20 Y. Yao, B. Gao, H. Chen, L. Jiang, M. Inyang, A. R. Zimmerman, X. Cao, L. Yang, Y. Xue and H. Li, *J. Hazard. Mater.*, 2012, **209-210**, 408-413.

21 C. Fang, T. Zhang, P. Li, R. Jiang, S. Wu, H. Nie and Y. Wang, *J. Environ. Sci.*, 2015, **29**, 106-114.

22 Y. Chun, G. Sheng, C. T. Chiou and B. Xing, *Environ. Sci. Technol.*, 2004, **38**, 4649-4655.

23 G. N. Kasozi, A. R. Zimmerman, P. Nkedi-Kizza and B. Gao, *Environ. Sci. Technol.*, 2010, **44**, 6189-6195.

24 L. Beesley, E. Moreno-Jiménez, J. L. Gomez-Eyles, E. Harris, B. Robinson and T. Sizmur, *Environ. Pollut.*, 2011, **159**, 3269-3282.

25 M. Inyang, B. Gao, Y. Yao, Y. Xue, A.R. Zimmerman, P. Pullammanappallil and X. Cao, *Bioresour. Technol.*, 2012, **110**, 50-56.

26 M. Zhang, B. Gao, Y. Yao, Y. Xue and M. Inyang, *Sci. Total Environ.*, 2012, **435-436**, 567-572.

27 Y. Xue, B. Gao, Y. Yao, M. Inyang, M. Zhang, A. R. Zimmerman and K. S. Ro, *Chem. Eng. J.*, 2012, **200-202**, 673-680.

28 Z. Wang, H. Guo, F. Shen, G. Yang, Y. Zhang, Y. Zeng, L. Wang, H. Xiao and S. Deng, *Chemosphere*, 2015, **119**, 646-653.

29 A. Mukherjee, A. R. Zimmerman and W. Harris, *Geoderma*, 2011, **163**, 247-255.

30 C. Namasivayam and D. Sangeetha, *J. Colloid Interface Sci.*, 2004, **280**, 359-365.

31 B. Chen, Z. Chen and S. Lv, *Bioresour. Technol.*, 2011, **102**, 716-723.

32 M. Zhang and B. Gao, *Chem. Eng. J.*, 2013, **226**, 286-292.

33 Y. Liu, H. Li, G. Q. Tan and X. H. Zhu, *Sep. Sci. Technol.*, 2010, **46**, 290-299.

34 J. H. Yuan, R. K. Xu and H. Zhang, *Bioresour. Technol.*, 2011, **102**, 3488-3497.

35 N. Y. Mezenner and A. Bensmaili, *Chem. Eng. J.*, 2009, **147**, 87-96.

36 J. Murphy and J. P. Riley, *Anal. Chim. Acta.*, 1962, **27**, 31-36.

37 N. Venkatathri, R. Srivastava, D. S. Yun and J. W. Yoo, *Microporous Mesoporous Mater.*, 2008, **112**, 147-152.

38 E. Repo, J. K. Warchoł, A. Bhatnagar and M. Sillanpää, *J. Colloid Interface Sci.*, 2011, **358**, 261-267.

39 K. Dimos, P. Stathi, M. A. Karakassides and Y. Deligiannakis, *Microporous Mesoporous Mater.*, 2009, **126**, 65-71.

40 L. Yue, Y. Zheng and D. Jin, *Microporous Mesoporous Mater.*, 2008, **113**, 538-541.

41 I. de Vicente, A. Merino-Martos, L. Cruz-Pizarro and J. de Vicente, *J. Hazard. Mater.*, 2010, **181**, 375-381.

42 W. Y. Huang, D. Li, J. Yang, Z. Q. Liu, Y. Zhu, Q. Tao, K. Xu, J. Q. Li and Y. M. Zhang,

Microporous Mesoporous Mater., 2013, **170**, 200-210.

43 C. Gan, Y. G. Liu, X. F. Tan, S. F. Wang, G. M. Zeng, B. H. Zheng, T. T. Li, Z. J. Jiang and W. Liu, *RSC Adv*., 2015, **5**, 35107-35115.

44 D. J. Wang, W. Zhang, X. Z. Hao and D. M. Zhou, *Environ. Sci. Technol.*, 2013, **47**, 821-828.

45 M. Essandoh, B. Kunwar, C. U. Pittman Jr, D. Mohan and T. Mlsna, *Chem. Eng. J.*, 2015, **265**, 219-227.41.

46 F. C. Wu, R. L. Tseng and R. S. Juang, *J. Hazard. Mater.*, 2001, **81**, 167-177.

47 H. Lu, W. Zhang, Y. Yang, X. Huang, S. Wang and R. Qiu, *Water Res.*, 2012, **46**, 854-862.

48 M. Li, Q. Liu, L. Guo, Y. Zhang, Z. Lou, Y. Wang and G. Qian, *Bioresour. Technol.*, 2013, **141**, 83-88.

49 J. Zhang, Z. Shen, W. Shan, Z. Chen, Z. Mei, Y. Lei and W. Wang, *J. Environ. Sci.*, 2010, **22**, 507-511.

50 Q. Zhou, X. Wang, J. Liu and L. Zhang, *Chem. Eng. J.*, 2012, **200-202**, 619-626.

51 S. Y. Yoon, C. G. Lee, J. A. Park, J. H. Kim, S. B. Kim, S. H. Lee and J. W. Choi, *Chem. Eng. J.*, 2014, **236**, 341-347.

52 L. V. A. Gurgel and L. F. Gil, *Water Res.*, 2009, **43**, 4479-4488.

53 R. S. Juang, F. C. Wu and R. L. Tseng, *Water Res.*, 1999, **33**, 2403-2409.

54 Y. Gao, L. E. E. Kyue-Hyung, M. Oshima and S. Motomizu, *Anal. Sci.*, 2000, **16**, 1303-1308.

55 G. Li, S. Gao, G. Zhang and X. Zhang, *Chem. Eng. J.*, 2014, **235**, 124-131.

56 H. Li, J. Ru, W. Yin, X. Liu, J. Wang and W. Zhang, *J. Hazard. Mater.*, 2009, **168**, 326-330.

57 H. Liu, X. Sun, C. Yin and C. Hu, *J. Hazard. Mater.*, 2008, **151**, 616-622.

58 Y. Yao, B. Gao, M. Inyang, A. R. Zimmerman, X. Cao, P. Pullammanappallil and L. Yang, *J. Hazard. Mater.*, 2011, **190**, 501-507.59 L. Tang, G. D. Yang, G. M. Zeng, Y. Cai, S. S. Li, Y. Y. Zhou, Y. Pang, Y. Y. Liu, Y. Zhang and B. Luna, *Chem. Eng. J.*, 2014, **239**, 114-122.

60 Q. Z. Chen, I. D. Thompson and A. R. Boccaccini, *Biomaterials*, 2006, **27**, 2414-2425.

61 C. R. Kothapalli M. T. Shaw and M. Wei, *Acta Biomater.*, 2005, **1**, 653-662.

62 D. Arcos and M. Vallet-Regí, *Acta Biomater*., 2010, **6**, 2874-2888.

63 P. Galindo-Moreno, G. Ávila, J. E. Fernández-Barbero, F. Mesa, F. O'Valle-Ravassa and H. L. Wang, *Clin. Oral. Implants Res*., 2008, **19**, 755-759.

64 M. Padial-Molina, P. Galindo-Moreno and G. Avila-Ortiz, *Minerva Biotechnol*., 2009, **21**, 173-186.

65 Y. H. Li, K. Y. Li, M. Su, Y. M. Ren, Y. Li, J. X. Chen and L. Li, *Carbohyd. Polym.*, 2016, **153**, 320-328.

66 D. Chen, Z. Y. Zeng, Y. B. Zeng, F. Zhang and M. Wang, *Water Resources and Industry*, 2016, **15**, 1-13.

Table 1 Kinetic parameters for the adsorption of phosphate on biochars, based on the pseudo-first-order and pseudo-second-order kinetic models

Sample	Initial concentration ($mg \cdot L^{-1}$)	Experimental parameters		Pseudo-first order			Pseudo-second order		
		pH	$q_{e,exp}$ ($mg \cdot g^{-1}$)	k_1 (min^{-1})	$q_{e,cal}$ ($mg \cdot g^{-1}$)	R^2	k_2 ($g \cdot mg^{-1} \cdot min^{-1}$)	$q_{e,cal}$ ($mg \cdot g^{-1}$)	R^2
BC	10	5	8.6	0.0029	1.11	0.8861	0.012	8.62	0.999
VBC	10	5	9.80	0.0041	2.49	0.968	0.0056	9.89	0.999
BC	50	5	46.70	0.00033	3.80	0.442	0.0029	46.86	0.999
VBC	50	5	49.70	0.0028	4.36	0.335	0.0027	49.72	0.999

Table 2 Langmuir, Freundlich, and Redlich-Peterson parameters for phosphate adsorption on BC and VBC

Sample	Langmuir constants			Freundlich constants			Redlich-Peterson constants			
	K_L ($mg \cdot g^{-1}$)	b	R^2	K_F $(mg/g)(L/mg)^{1/n}$	n	R^2	K_R ($L \cdot g^{-1}$)	a_R $(L/mg)^{1/n}$	B	R^2
BC	98.20	0.1015	0.9768	11.24	1.717	0.9548	3.177	-4.746×10^{7}	-3.575×10^{6}	0.7577
VBC	159.42	0.3077	0.9789	34.62	1.508	0.9550	8.61×10^{-4}	-0.999	-7.65×10^{-6}	0.9172

Table 3 Comparison of maximum phosphate adsorption capacities for different adsorbents

Adsorbents	Equilibrium Conc. ($mg \cdot L^{-1}$)	Maximum adsorption capacity ($mg \cdot g^{-1}$)	Reference
Fe–Cu binary oxide	0–25	39.80	55
La-doped vesuvianite	0–4	6.70	56
Mesoporous ZrO_2	0–275	29.70	57
ACF-NanoHFO	5–40	12.86	50
Biochar/AlOOH nanocomposite	0–120	135.00	32
Magnetic iron oxide nanoparticles	2–20	5.03	51
Biochar derived from digested sugar beet tailings	15–640	133.09	58
BC	2–100	98.20	Present work
VBC	2–100	159.40	Present work

Figure Captions

Fig. 1 XRD pattern (a) and FT-IR spectrum (b) of vermiculite-modified biochar.

Fig. 2 FESEM images (a, b, and c) and the energy-dispersive X-ray (EDX) spectroscopic analysis (d) of vermiculite-modified biochar.

Fig. 3 Nitrogen adsorption-desorption isotherms (a) and pore size distribution (b) of BC and VBC.

Fig. 4 Effect of pH on the removal of phosphate by BC and VBC for 24 h at an initial concentration of 10 $mg \cdot L^{-1}$ (a) and 50 $mg \cdot L^{-1}$ (b).

Fig. 5 Zeta potentials of BC and VBC at different solution pH.

Fig. 6 Effect of contact time on the removal of phosphate at pH 5.0 by BC and VBC at an initial concentration of 10 $mg \cdot L^{-1}$ (a) and 50 $mg \cdot L^{-1}$ (b).

Fig. 7 Pseudo-first order kinetic sorption data (a and c) and pseudo-second order kinetic sorption data (b and d) for phosphate by BC (a and b) and VBC (c and d) at an initial concentration of 10 $mg \cdot L^{-1}$.

Fig. 8 Pseudo-first order kinetic sorption data (a and c) and pseudo-second order kinetic sorption data (b and d) for phosphate by BC (a and b) and VBC (c and d) at an initial concentration of 50 $mg \cdot L^{-1}$.

Fig. 9 Comparison of Langmuir, Freundlich, and Redlich-Peterson isotherms for the phosphate adsorption onto BC (a) and VBC (b).

Fig. 10 Effect of different concentrations of NaCl on phosphate removal by VBC.

Fig. 11 Effect of coexisting anions on phosphate adsorption onto VBC.

Fig. 12 Fifth consecutive adsorption–desorption cycle of VBC for phosphate removal (a) and FESEM image of VBC after fifth adsorption–desorption cycle (b).

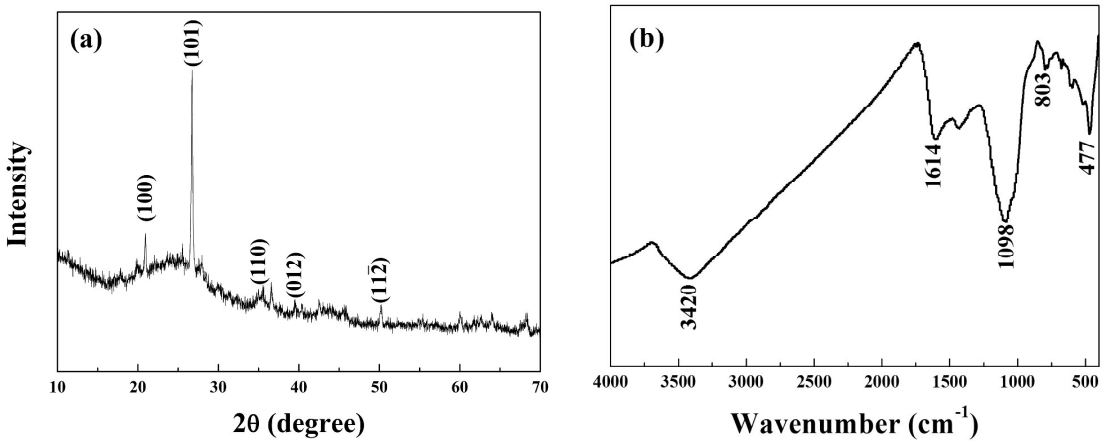

Figure 1

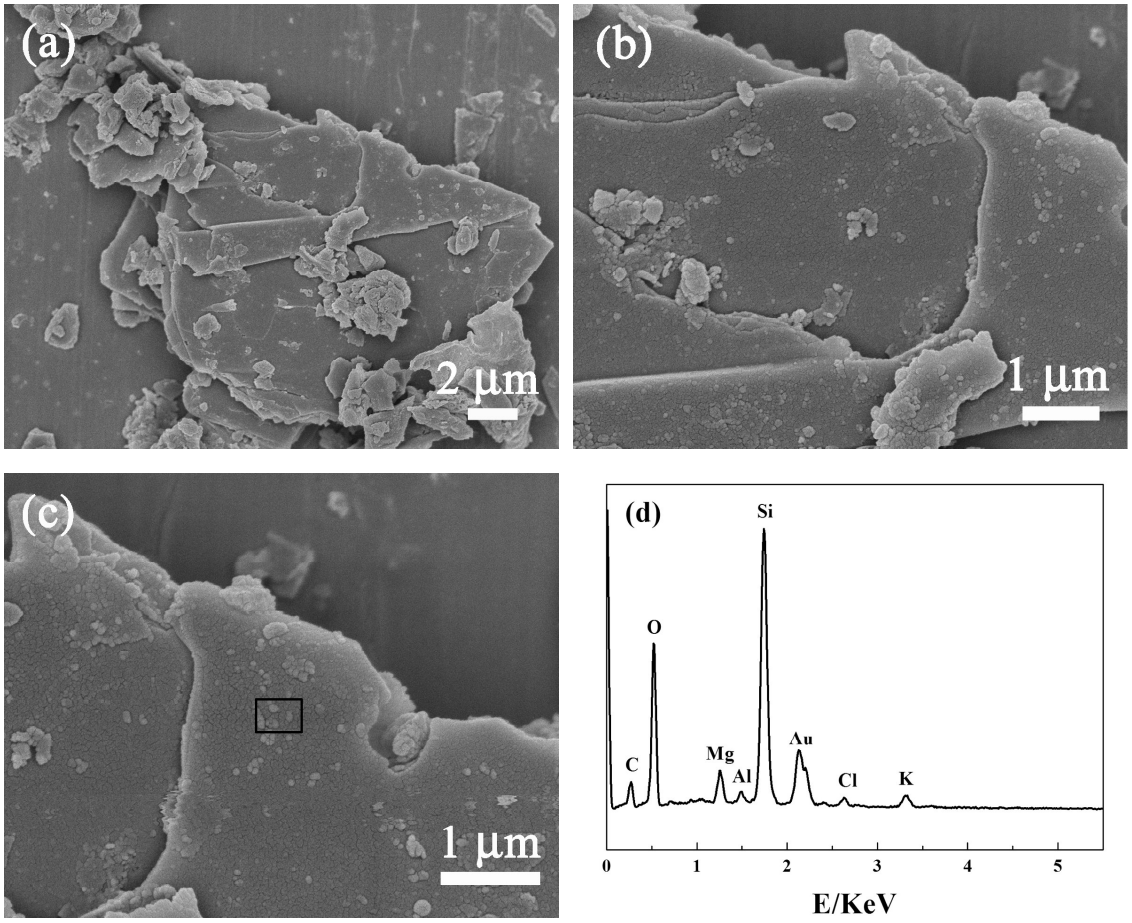

Figure 2

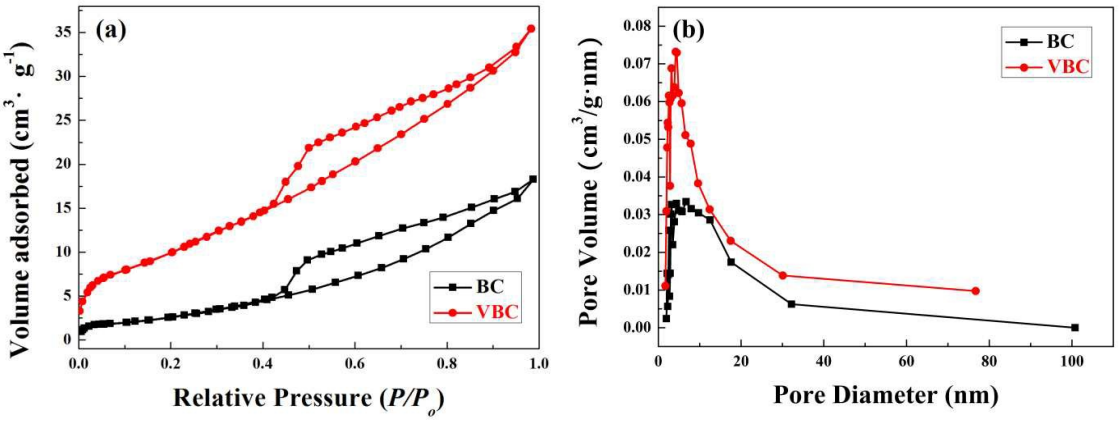

Figure 3

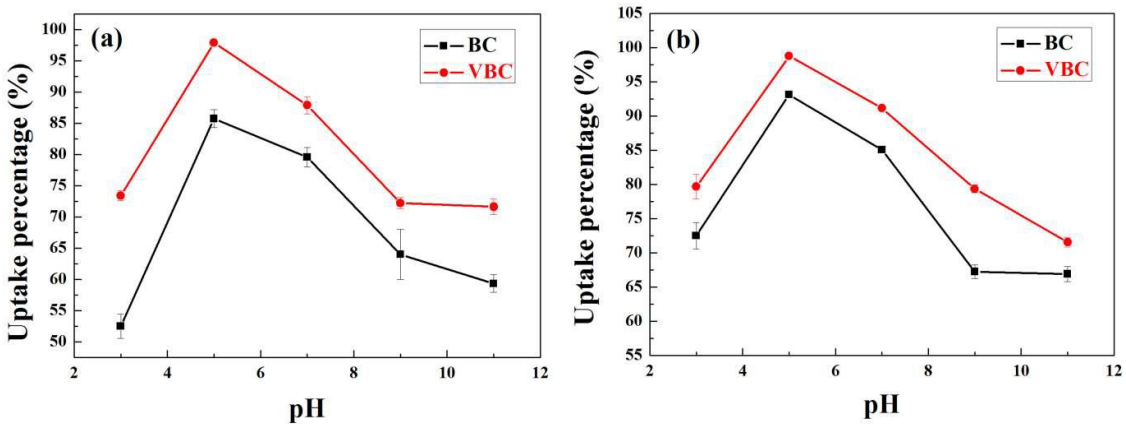

Figure 4

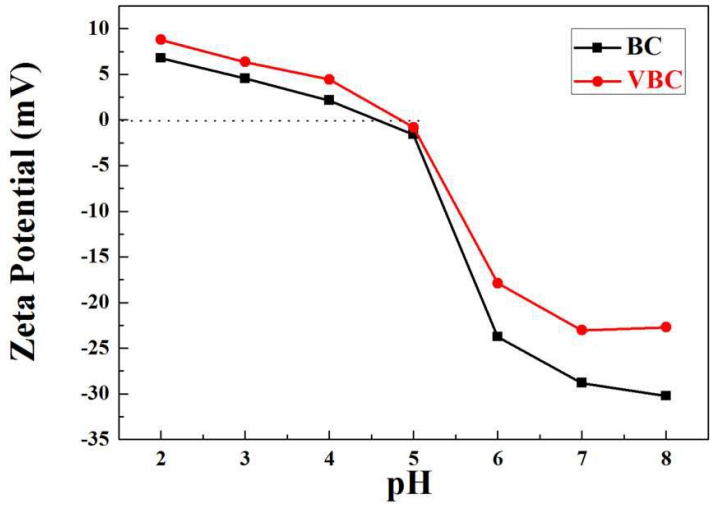

Figure 5

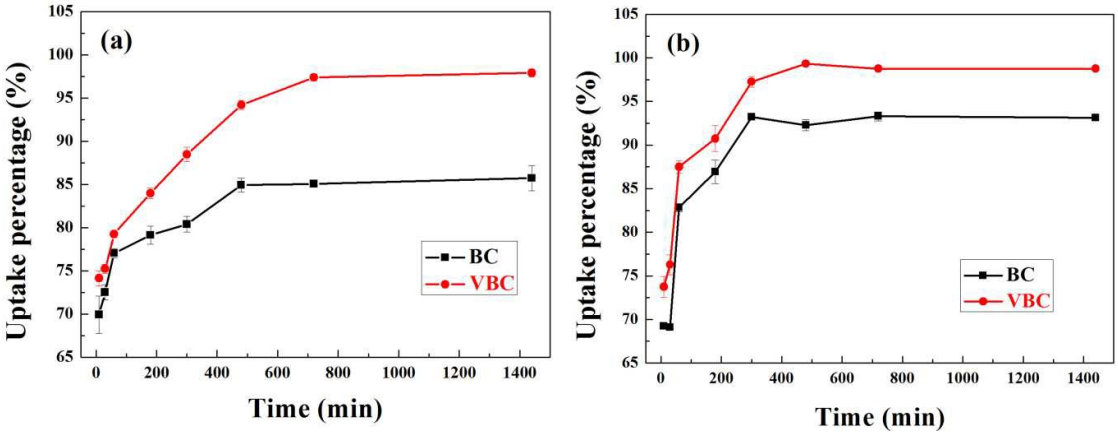

Figure 6

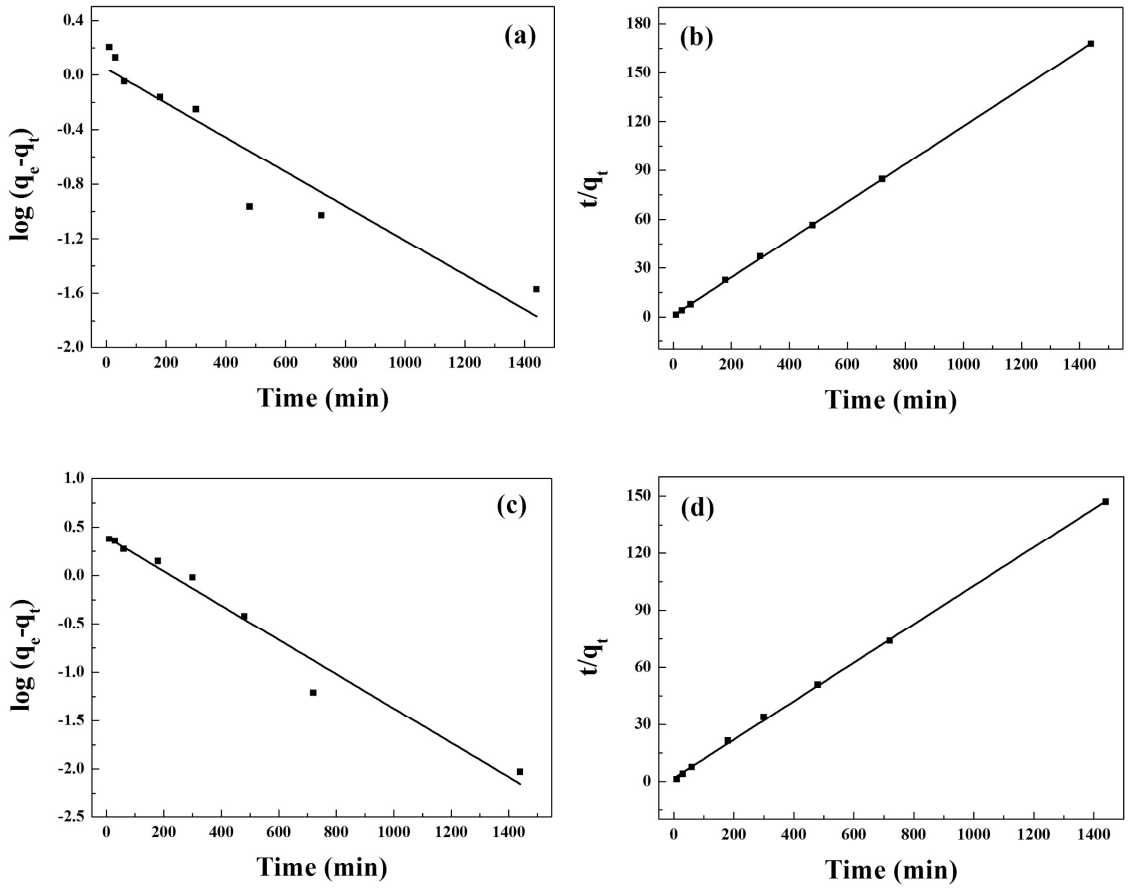

Figure 7

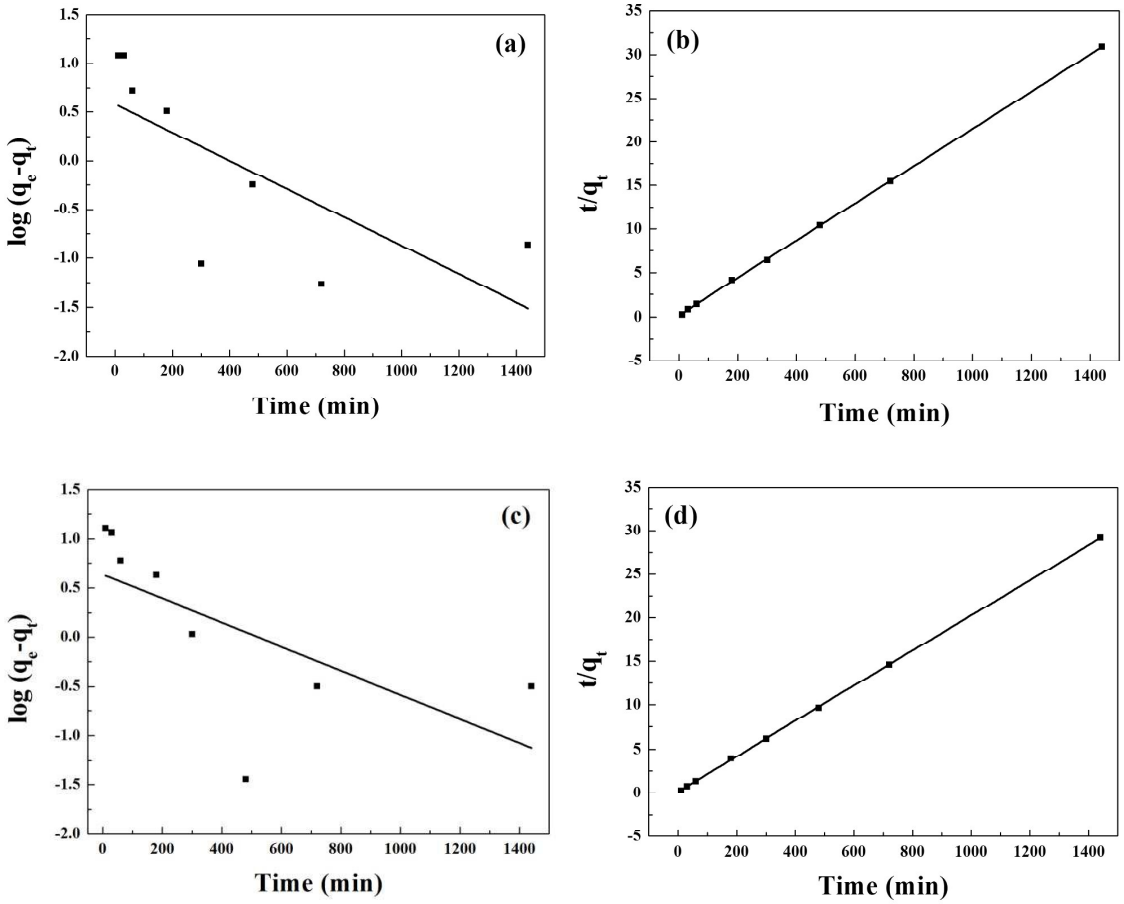

Figure 8

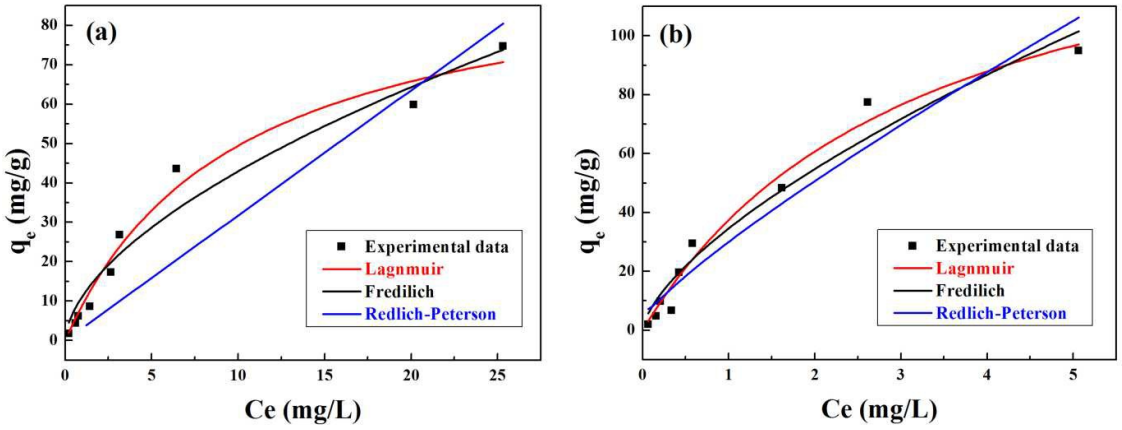

Figure 9

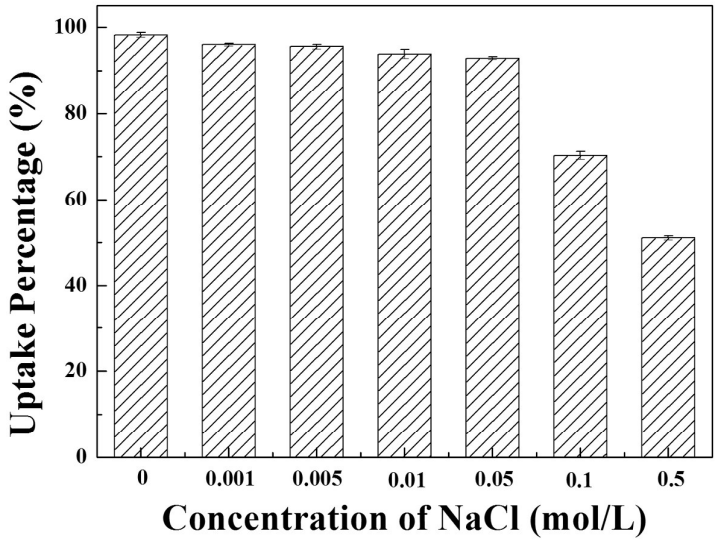

Figure 10

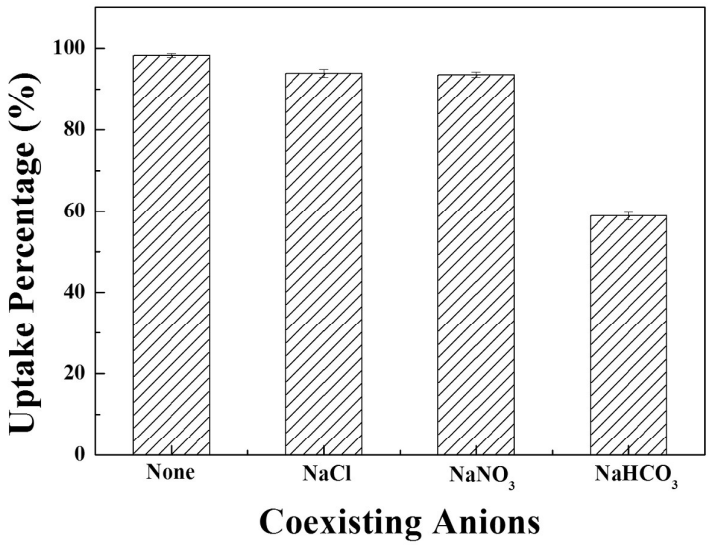

Figure 11

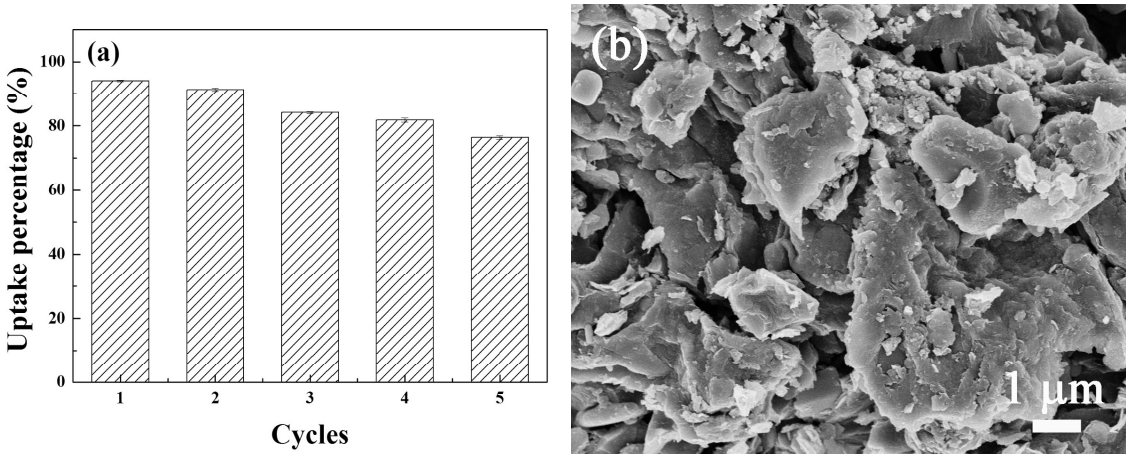

Figure 12